

Investigation of the AFM Indenter's Geometry Effect On Micro/Nano Biological Cells' Indentation

Yousef Habibi Sooha¹, Moharam Habibnejad Korayem^{2, *}, Zahra Rastegar³

Department of Mechanical Engineering,
Iran University of Science and Technology
Yousefsooha.iust@gmail.com, hkorayem@iust.ac.ir,
Za_Rastegar@mecheng.iust.ac.ir

*Corresponding author

Received: 11 February 2018 Revised: 13 March 2018, Accepted: 20 May 2018

Abstract: The elasticity modules of the micro/Nanoparticles, especially biological particles are measured using different tools such as atomic force microscopy. The tip of the atomic force microscopy as an indenter has different shapes such as spherical, conical and pyramidal. In the contact of these tips and biological cells, avoiding the cell damage is a necessity. The goal of this paper is investigation and comparison of different tips' geometries. Different tip's geometries and their related theories were collected and proposed. To generalize theories' application for any kind of particle (even non-biological particles) some of simplifying assumptions used in these theories, such as tip rigidity, were removed. Simulation of the force-indentation depth was done for gold nanoparticle and observed that if simplifying assumptions were not removed there would be big errors in calculating the elasticity module of some particles. Then, simulations were done for two yeast and mouse embryo cells. For both cells, in general, the geometry of the curve group, the geometry of the pyramidal group and finally the geometry of the conical group were positioned from the highest to the lowest places. For hyperbolic, conical and pyramidal tips, the important parameter was semi vertical angel. To observe its effect, different magnitudes of this parameter were simulated. According to observed results in three investigated geometries and for both cells, bigger semi vertical angel created higher curves and this means in bigger angels the possibility of cell damage is higher.

Keywords: Atomic Force Microscopy, Biological Cell Damage, Elasticity Module, Tip Geometry

Reference: Yousef Habibi sooha, Moharam Habibnejad Korayem, and Zahra Rastegar, "Investigation of the AFM Indenter's Geometry Effect On Micro/Nano Biological Cells", Int J of Advanced Design and Manufacturing Technology, Vol. 13/No. 4, 2020, pp. 99–108. DOI: 10.30495/admt.2021.560583.1019

Biographical notes: **Yousef Habibi Sooha** received his BSc degree in mechanical engineering and MSc degree in Biomechanical Engineering from Iran University of Science and Technology, in 2014 and 2016 respectively. His current research interests include cell and tissue engineering and trauma. **Moharam Habibnejad Korayem** is a Professor in Mechanical Engineering at Iran University of Science and Technology. His research interests include dynamics of elastic mechanical manipulators, trajectory optimization, symbolic modeling, robotic multimedia software, mobile robots, industrial robotics standard, robot vision, soccer robot and the analysis of mechanical manipulator with maximum load carrying capacity. He has published more than 600 papers in international journal and conference in the robotic area. **Zahra Rastegar** received her BSc in Mechanical Engineering from the Ferdowsi University of Mashhad, and her MSc and PhD in Mechanical Engineering from Iran University of Science and Technology.

1 INTRODUCTION

According to the possibility of the cell damage during manipulation by atomic force microscopy, the contact moment is of great importance. Since the tip- particle contact depends on the tip and particle's geometry and material, the theory considers these parameters which can help solving the problem more accurately.

In recent decades, investigations about the cell biomechanics have been progressed significantly and different tools have been used [1]. Among these methods, atomic force microscopy was more interesting. Using cantilevers as soft Nano indenters makes it possible to test on small and heterogeneous samples such as cells and tissues [2-3]. Unlike general measurements, AFM has an indenter which is capable of a local Nano amplitude's mechanical properties measurement inside a single cell with lateral precision about Nano-meter in the liquid environment [4]. Different models are used to calculate the considered parameter, but most of them are based on Hertz model or extensible to experimental conditions which consider indenter geometry or sample thickness [5].

Nano mechanical analysis of biological cells are used increasingly in different fields such as cancer and evolutionary biology. There are differences between normal and abnormal cells' stiffness [6]. Determination of the salmon embryo cell's tension at three points of head, middle and end is one of the primary works in this field [7]. Also, according to existing organelles in cells and effect of their arrangement on cell properties, there was the probability of different properties at different points of the cell, therefore changes of the local elasticity module for Muller cells were investigated using AFM. Nano indentation tests on Muller cells were done at head, middle and end of them. Hertz standard model were applied to calculate elasticity module using force-indentation curves. One measurement point was selected from each different morphological region of the cell [8]. Studies were not only about biological cells but also included internal components such as collagen and determination of their mechanical properties [9]. The potential of the AFM in particles' Characterization has been used extensively in the biological materials' field and also other materials such as metal Nanoparticles [10]. The investigation of the indentation by a pyramidal tip has been done and an approximate solution was proposed for the frictionless indentation on the elastic half-space by a pyramidal tip. The method was based on acceptable assumption of the stress distribution at contact region. The relation between the force and the indentation depth was obtained for this problem and compared with numerical results [11]. The effect of the indenter geometry on the elastic body's response to the indentation was investigated in a research including different analytical solutions. Indentation of five

different tip geometries including spherical, cylindrical, and conical with obvious semi-vertical angle, Vickers pyramidal and Berkovich pyramidal on an elastomer was studied [12].

In a different research by Akhremitchev and Walker, the effect of the sample thickness, indented by the AFM, on the elasticity determination was investigated. They concluded that ignoring the sample thickness can significantly affect elasticity properties [13]. The similar work was done for determination of the polyvinyl alcohol gel thin layer's elasticity module using atomic force microscopy [14]. Thin samples and adherent cells' elasticity modules using atomic force microscopy were determined [15]. Rico et al. investigated live cells' mechanical properties indented by a blunted pyramidal cantilever tip of the AFM [16]. Although conventional indentation by AFM suffers from high stress by its sharp tip, to solve this problem spherical tips with the controlled non-destructive stress have been used [17]. However, there is a lack of a comprehensive research studies on the effect of different tip geometries. In this paper, numerical simulations results are considerable. Since existing theories have used some simplifying assumptions, they need some corrections to be applicable for all kinds of particles (even biological cells), which have been done in following sections. Then different tip geometries, biological cell, and finally effective geometrical parameters of tips and samples have been investigated simultaneously to find out which tip and geometry has less destructive effect on the biological particle.

2 THEORY

In most equations extracted from references, the AFM tip has been considered rigid in comparison with the sample. The sample used in this paper is biological. According to the "Fig. 1", it is obvious that the tip in comparison with the biological cell does not have higher module necessarily, for example, collagen protein's module is in the order of *Gpa*.

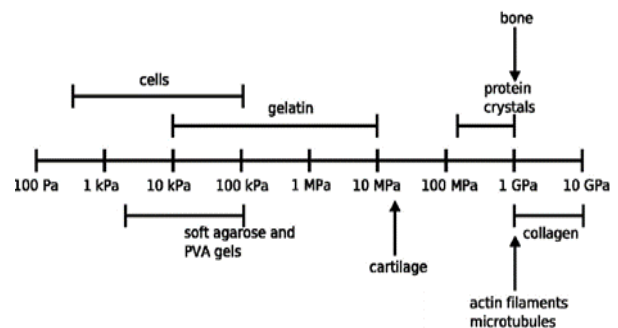


Fig. 1 Overall view to different biological cells' elasticity modules [18].

To have more accurate results and generalizing equations for all kinds of particles, it is better to consider the tip as an elastic material and apply its effect on the formulation. On the other hand, these formulations have been developed for the case in which sample radius is much bigger than tip radius. We know that some particles such as virus are in Nanoscale. Therefore, in all sections some corrections have been made on original formulations to apply the assumption of the elastic tip and consideration of the particle radius. Contact happens between the tip and the biological particle with radii of R_t and R_p . The contact radius is shown by a . Effective radius and elasticity module are defined by “Eqs. (1) and (2)”, [19-20]:

$$R = \left(\frac{1}{R_t} + \frac{1}{R_p} \right)^{-1} \quad (1)$$

$$E^* = \left(\frac{1-\nu_t^2}{E_t} + \frac{1-\nu_p^2}{E_p} \right)^{-1} \quad (2)$$

In the following, indices p and t will be used for the particle and tip respectively. $E_{t,p}$ and $\nu_{t,p}$ are young module and Poison’s ratio, respectively. Two bodies in contact apply compressive force of P on each other making them close together and increasing the force leads to indentation depth of δ . Relations between indentation depth, force and contact radius for Hertz elastic theory will be as “Eqs. (3) and (4)”, [21]:

$$\delta = \frac{a^2}{R} \quad (3)$$

$$P = \frac{4E^* a^3}{3R} \quad (4)$$

In the Hertz contact theory, it is assumed that two elastic bodies in contact are spherical, but since the tip is not necessarily spherical here, Hertz theory relations should be corrected. Different geometries of tips will be studied and according to their geometries will be divided into three groups of curve, conical and pyramidal.

2.1. Curve

Corrected spherical tip:

Hertz theory is reliable for the small indentation depth. A little change on rigid tip and the assumption of the bigger radius for the sample leads to “Eqs. (5) and (6)”, [18]:

$$\delta = \frac{a}{2} \ln \frac{R_t+a}{R_t-a} \quad (5)$$

$$P = \frac{E_p}{1-\nu_p^2} \left[\frac{a^2+R_t^2}{2} \ln \frac{R_t+a}{R_t-a} - aR_t \right] \quad (6)$$

In general, above equations can be corrected as “Eqs. (7) and (8)”:

$$\delta = \frac{a}{2} \ln \frac{R+a}{R-a} \quad (7)$$

$$P = E^* \left[\frac{a^2+R^2}{2} \ln \frac{R+a}{R-a} - aR \right] = E^* a \left[\delta \left(1 + \frac{R^2}{a^2} \right) - R \right] \quad (8)$$

Spherical tip for the thin sample:

$$P = \frac{4E_p\sqrt{R_t}}{3(1-\nu_p^2)} \delta^{\frac{3}{2}} \left[1 - \frac{2\alpha}{\pi} \chi + \frac{4\alpha^2}{\pi^2} \chi^2 - \frac{8}{\pi^3} \left(\alpha^3 + \frac{4\pi^2}{15} \beta \right) \chi^3 + \frac{16\alpha}{\pi^4} \left(\alpha^3 + \frac{3\pi^2}{5} \beta \right) \chi^4 \right] \quad (9)$$

In which $\chi = \sqrt{R_t\delta}/h$, h is the thickness of the biological cell, “Fig. 2”. α and β are dependent on the adhesion of the sample to the substrate [14]. For a bonded sample:

$$\alpha = -0.347 \frac{3-2\nu_p}{1-\nu_p}$$

$$\beta = 0.056 \frac{5-2\nu_p}{1-\nu_p}$$

And for a not-bonded sample:

$$\alpha = - \frac{1.2876 - 1.4678\nu_p + 1.3442\nu_p^2}{1-\nu_p}$$

$$\beta = \frac{0.6387 - 1.0277\nu_p + 1.5164\nu_p^2}{1-\nu_p}$$

Considering the corrected form of the $\chi' = \sqrt{R\delta}/h = a/h$, general form of the above equation can be corrected as “Eq. (10)”:

$$P = \frac{4E^*\sqrt{R}}{3} \delta^{\frac{3}{2}} \left[1 - \frac{2\alpha}{\pi} \chi' + \frac{4\alpha^2}{\pi^2} \chi'^2 - \frac{8}{\pi^3} \left(\alpha^3 + \frac{4\pi^2}{15} \beta \right) \chi'^3 + \frac{16\alpha}{\pi^4} \left(\alpha^3 + \frac{3\pi^2}{5} \beta \right) \chi'^4 \right] \quad (10)$$

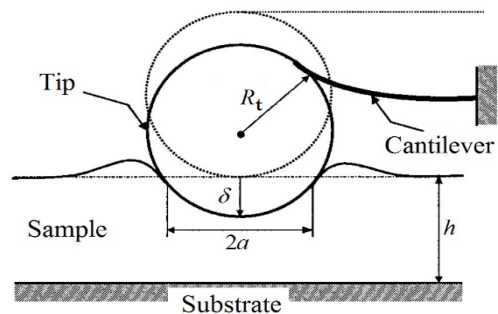


Fig. 2 Contact between spherical tip and the thin sample’s surface [14].

Hyperbolic:

$$\delta = \frac{a^2}{2R_t} \xi \left(\frac{\pi}{2} + \tan^{-1} \left[\frac{1}{2\xi} - \frac{\xi}{2} \right] \right) \quad (11)$$

$$P = \frac{E_p a^3}{(1-\nu_p^2)R_t} \left[\xi^2 + \frac{\xi}{2} (1 - \xi^2) \left(\frac{\pi}{2} + \tan^{-1} \left[\frac{1}{2\xi} - \frac{\xi}{2} \right] \right) \right] \quad (12)$$

In which, $\xi = R_t \cot \theta / a$ [13]. Corrected form of two above equations considering $\xi' = R \cot \theta / a$ will be as follows:

$$\delta = \frac{a^2}{2R} \xi' \left(\frac{\pi}{2} + \tan^{-1} \left[\frac{1}{2\xi'} - \frac{\xi'}{2} \right] \right) \quad (13)$$

$$P = \frac{E^* a^3}{R} \left[\xi'^2 + \frac{\xi'}{2} (1 - \xi'^2) \left(\frac{\pi}{2} + \tan^{-1} \left[\frac{1}{2\xi'} - \frac{\xi'}{2} \right] \right) \right] \quad (14)$$

Parabolic:

$$\delta = \frac{a^2}{R_t} \quad (15)$$

$$P = \frac{4E_p a^3}{3(1-\nu_p^2)R_t} \quad (16)$$

The corrected form of which is as “Eqs. (3) and (4)”, [13-14]. (“Fig. 3”)

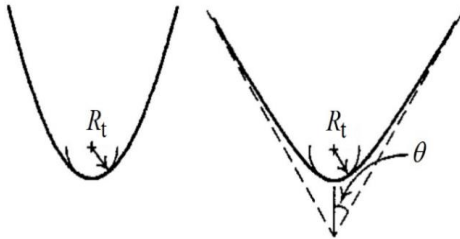


Fig. 3 Hyperbolic tip (left) and parabolic tip (right) [13].

2.2. Conical**Conical:**

Indentation depth and force equations are [18], “Fig. 4” [22-23]:

$$\delta = \frac{\pi}{2 \tan \theta} a \quad (17)$$

$$P = \frac{2E_p \tan \theta}{\pi(1-\nu_p^2)} \delta^2 \quad (18)$$

The corrected form of which is as “Eq. (19)”:

$$P = \frac{2E^* \tan \theta}{\pi} \delta^2 \quad (19)$$

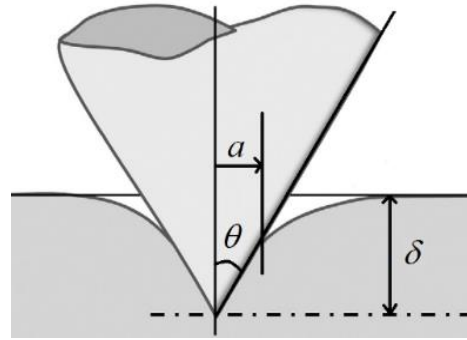


Fig. 4 Contact of the conical tip and the sample [23].

Conical tip and the thin sample:

$$P = \frac{2E_p \tan \theta}{3\pi} \delta^2 \left[1 + \varphi \frac{2 \tan \theta}{\pi^2 h} \delta + \varphi^2 \frac{16 \tan^2 \theta}{h^2} \delta^2 \right] \quad (20)$$

For adherent particles $\varphi = 1.7795$ and for non-adherent particles $\varphi = 0.388$ [15]. So:

$$P = \frac{2(1-\nu_p^2)E^* \tan \theta}{3\pi} \delta^2 \left[1 + \varphi \frac{2 \tan \theta}{\pi^2 h} \delta + \varphi^2 \frac{16 \tan^2 \theta}{h^2} \delta^2 \right] \quad (21)$$

Blunted conical tip:

Hertz solution is used for small indentations of the sphere, in which contact radius is less than effective radius [12]. For bigger indentations:

$$\delta = \frac{a}{\tan \theta} \left(\frac{\pi}{2} - \sin^{-1} \left[\frac{b}{a} \right] \right) - \frac{a}{R_t} [\sqrt{a^2 - b^2} - a] \quad (22)$$

$$P = \frac{2E_p}{(1-\nu_p^2)} \left[a\delta - \frac{a^2}{2 \tan \theta} \left(\frac{\pi}{2} - \sin^{-1} \left[\frac{b}{a} \right] \right) - \frac{a^3}{3R_t} + \sqrt{a^2 - b^2} \left(\frac{b}{2 \tan \theta} + \frac{a^2 - b^2}{3R_t} \right) \right] \quad (23)$$

When $b = 0$ “Eqs. (22) and (23)” will be converted to complete conical tip’s equations- “Eqs. (17) and (18)”. When $b = a$, above equations are converted to cylindrical tip’s equations which will be studied in the following sections. When the spherical tip is connected to the conical body continuously and tangentially, the equation $b = R \cos \theta$ will be used. Corrected equations will be as follows:

$$\delta = \frac{a}{\tan \theta} \left(\frac{\pi}{2} - \sin^{-1} \left[\frac{b}{a} \right] \right) - \frac{a}{R} [\sqrt{a^2 - b^2} - a] \quad (24)$$

$$P = 2E^* \left[a\delta - \frac{a^2}{2 \tan \theta} \left(\frac{\pi}{2} - \sin^{-1} \left[\frac{b}{a} \right] \right) - \frac{a^3}{3R} + \sqrt{a^2 - b^2} \left(\frac{b}{2 \tan \theta} + \frac{a^2 - b^2}{3R} \right) \right] \quad (25)$$

Truncated cone:

Truncated cone can be considered as a special kind of blunted cone in which the curvature radius is infinite at the tip [12]. Substituting $R_t = \infty$ in blunted head cone's equations we will have:

$$\delta = \frac{a}{\tan \theta} \left(\frac{\pi}{2} - \sin^{-1} \left[\frac{b}{a} \right] \right) \quad (26)$$

$$P = \frac{2E_p}{(1-\nu_p^2)} \left[a\delta - \frac{a^2}{2 \tan \theta} \left(\frac{\pi}{2} - \sin^{-1} \left[\frac{b}{a} \right] \right) + \sqrt{a^2 - b^2} \left(\frac{b}{2 \tan \theta} \right) \right] \quad (27)$$

And the corrected form of "Eqs. (24) and (25)" will be as:

$$\delta = \frac{a}{\tan \theta} \left(\frac{\pi}{2} - \sin^{-1} \left[\frac{b}{a} \right] \right) - \frac{a}{R_c} [\sqrt{a^2 - b^2} - a] \quad (28)$$

$$P = 2E^* \left[a\delta - \frac{a^2}{2 \tan \theta} \left(\frac{\pi}{2} - \sin^{-1} \left[\frac{b}{a} \right] \right) - \frac{a^3}{3R_c} + \sqrt{a^2 - b^2} \left(\frac{b}{2 \tan \theta} + \frac{a^2 - b^2}{3R_c} \right) \right] \quad (29)$$

Cylindrical:

Force- indentation depth equation for a cylindrical indenter is as "Eq. (30)", [23]:

$$P = 2E^* r \delta \quad (30)$$

2.3. Pyramid

Regular tetragonal pyramid:

$$\delta = \frac{\sqrt{2}a}{\tan \theta} \quad (31)$$

$$P = \frac{E_p \tan \theta}{\sqrt{2}(1-\nu_p^2)} \delta^2 \quad (32)$$

The corrected form of which will be as [12], [16], [18]:

$$P = \frac{E^* \tan \theta}{\sqrt{2}} \delta^2 \quad (33)$$

Blunted regular tetragonal pyramid:

As blunted head cone the blunted regular tetragonal pyramid can be created [16]:

$$\delta = \frac{2\sqrt{2}a}{\pi \tan \theta} \left(\frac{\pi}{2} - \sin^{-1} \left[\frac{b}{a} \right] \right) - \frac{a}{R_t} [\sqrt{a^2 - b^2} - a] \quad (34)$$

$$P = \frac{2E_p}{(1-\nu_p^2)} \left[a\delta - \frac{\sqrt{2}a^2}{\pi \tan \theta} \left(\frac{\pi}{2} - \sin^{-1} \left[\frac{b}{a} \right] \right) - \frac{a^3}{3R_t} + \sqrt{a^2 - b^2} \left(\frac{\sqrt{2}b}{\pi \tan \theta} + \frac{a^2 - b^2}{3R_t} \right) \right] \quad (35)$$

So, we have:

$$\delta = \frac{2\sqrt{2}a}{\pi \tan \theta} \left(\frac{\pi}{2} - \sin^{-1} \left[\frac{b}{a} \right] \right) - \frac{a}{R} [\sqrt{a^2 - b^2} - a] \quad (36)$$

$$P = 2E^* \left[a\delta - \frac{\sqrt{2}a^2}{\pi \tan \theta} \left(\frac{\pi}{2} - \sin^{-1} \left[\frac{b}{a} \right] \right) - \frac{a^3}{3R} + \sqrt{a^2 - b^2} \left(\frac{\sqrt{2}b}{\pi \tan \theta} + \frac{a^2 - b^2}{3R} \right) \right] \quad (37)$$

The contact of the tip and the sample surface is shown in "Fig. 5".

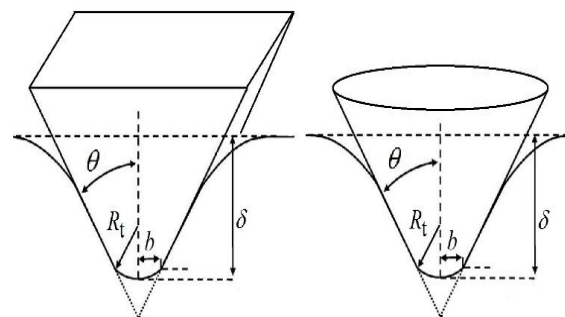


Fig. 5 The contact of the tip and the sample surface: blunted regular tetragonal pyramidal tip (left), blunted head conical tip (right) [16].

Truncated regular tetragonal pyramid:

Truncated pyramid is a special condition of the blunted head in which curvature radius at the tip is infinite [16]. So:

$$\delta = \frac{2\sqrt{2}a}{\pi \tan \theta} \left(\frac{\pi}{2} - \sin^{-1} \left[\frac{b}{a} \right] \right) \quad (38)$$

$$P = \frac{2E_p}{(1-\nu_p^2)} \left[a\delta - \frac{\sqrt{2}a^2}{\pi \tan \theta} \left(\frac{\pi}{2} - \sin^{-1} \left[\frac{b}{a} \right] \right) + \sqrt{a^2 - b^2} \left(\frac{\sqrt{2}b}{\pi \tan \theta} \right) \right] \quad (39)$$

And the corrected form of "Eqs. (36) and (37)" will be as follows:

$$\delta = \frac{2\sqrt{2}a}{\pi \tan \theta} \left(\frac{\pi}{2} - \sin^{-1} \left[\frac{b}{a} \right] \right) - \frac{a}{R_p} [\sqrt{a^2 - b^2} - a] \quad (40)$$

$$P = 2E^* \left[a\delta - \frac{\sqrt{2}a^2}{\pi \tan \theta} \left(\frac{\pi}{2} - \sin^{-1} \left[\frac{b}{a} \right] \right) - \frac{a^3}{3R_p} + \sqrt{a^2 - b^2} \left(\frac{\sqrt{2}b}{\pi \tan \theta} + \frac{a^2 - b^2}{3R_p} \right) \right] \quad (41)$$

3 SIMULATION AND RESULTS

In this section, simulations of three proposed classes of tip's geometries (curve, conical and pyramidal) will be done. These three theories have been proposed such a way that AFM tip in comparison with the sample considered is rigid. So, in the equation of the effective

elasticity module (equation 2), tip's module was not considered. Moreover, the effective radius was approximated by tip's radius because their radii were smaller in comparison with the sample (equation 1), the tips' radii were in Nanoscale but samples were in micro or even higher scales. As mentioned before, these two assumptions make considerable errors for particles with radii near the tip and high elasticity modules. So, ignoring these two assumptions, equations were proposed for more general condition. So, first the error rate made by these assumptions was investigated by the force-indentation depth simulation for gold nanoparticle, "Fig. 6". According to existing results in "Fig. 6", differences between corrected theories and previous ones are significant and proposed assumptions resulted in big errors for samples' elasticity module calculations and prediction of force-indentation depth curves.

Then, force-indentation depth simulations have been done for yeast and mouse embryonic cells, "Figs. 7 and 8". Yeast cell have an elasticity module in MPa scale but mouse embryonic cell's module is in the kilopascal range, "Table 1".

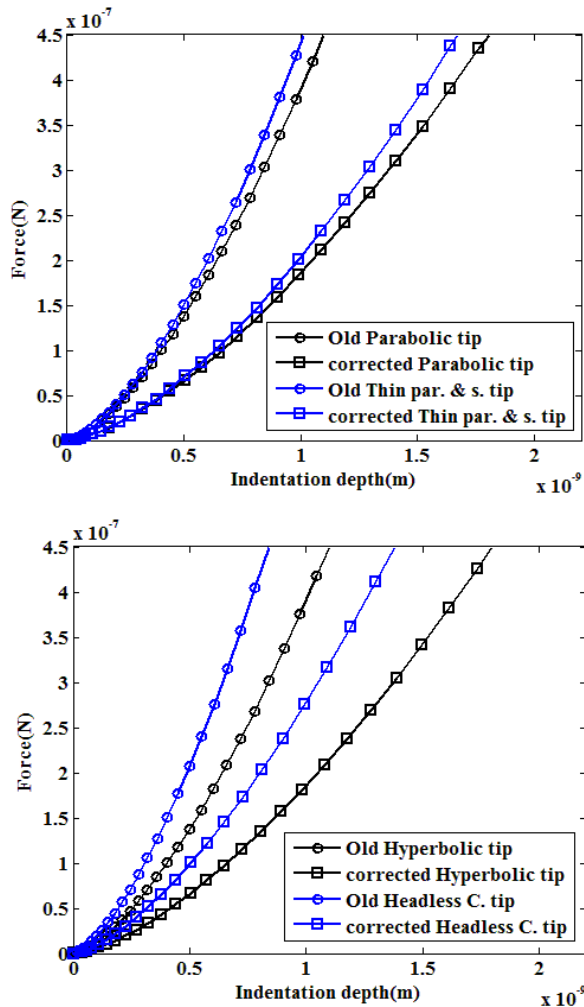
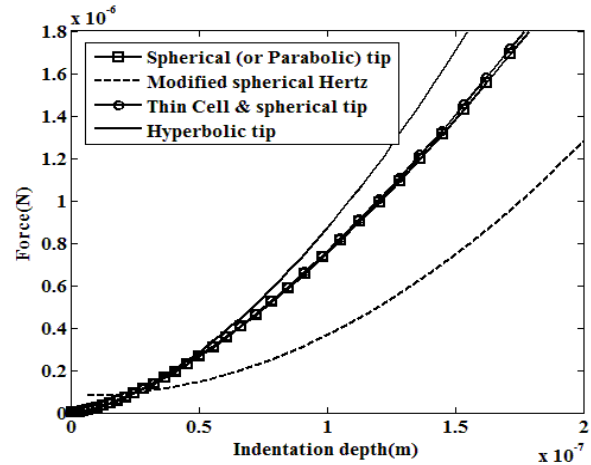
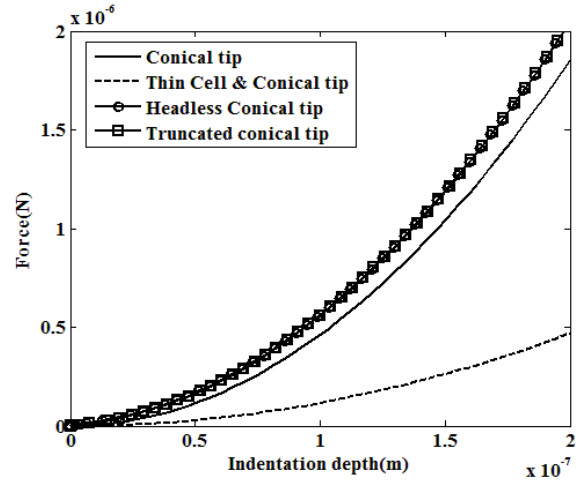


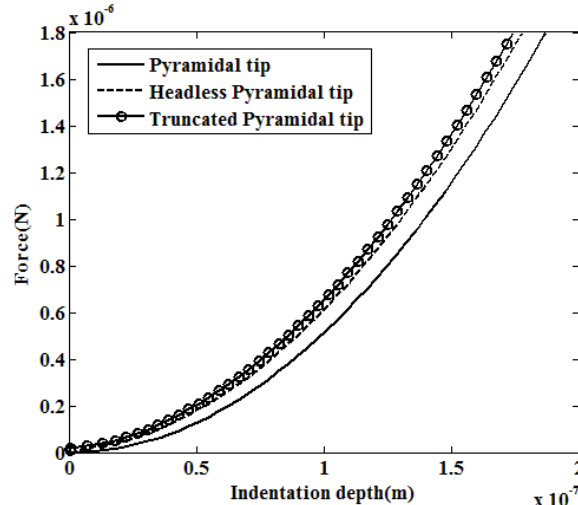
Fig. 6 Force-indentation depth simulation for gold Nano particle: study of the previous and new theories (corrected based on the effect of the all particles in contact).



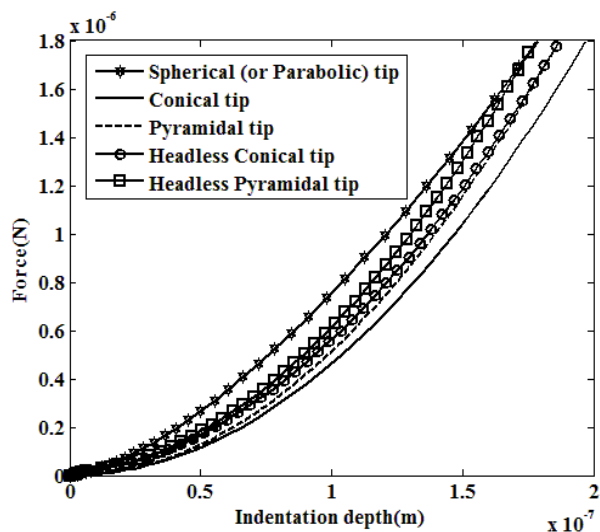
(a): Curve class



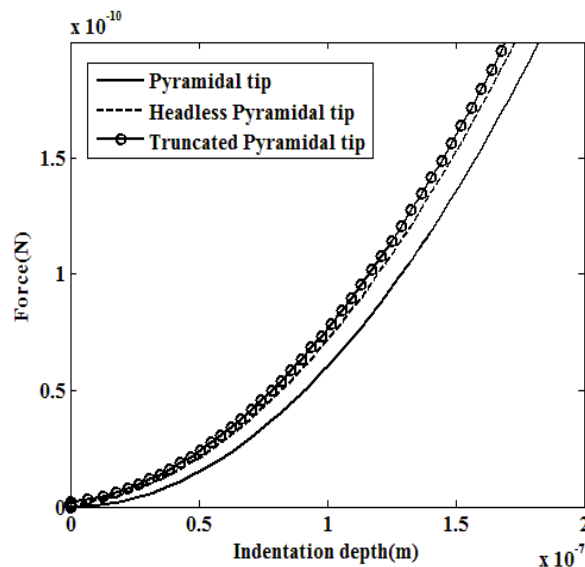
(b): Conical class



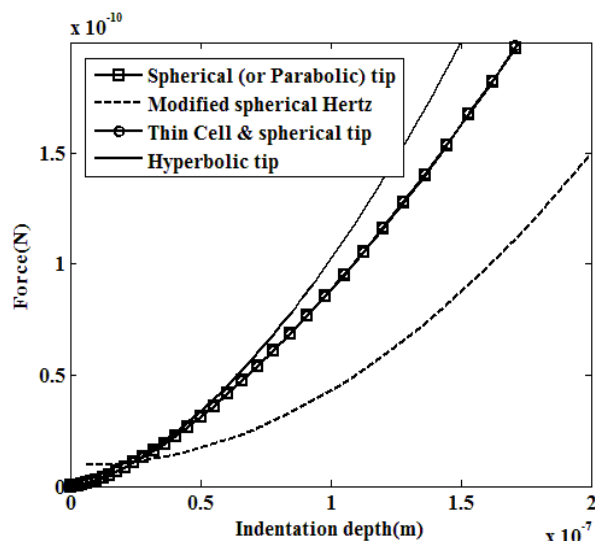
(c): Pyramidal class



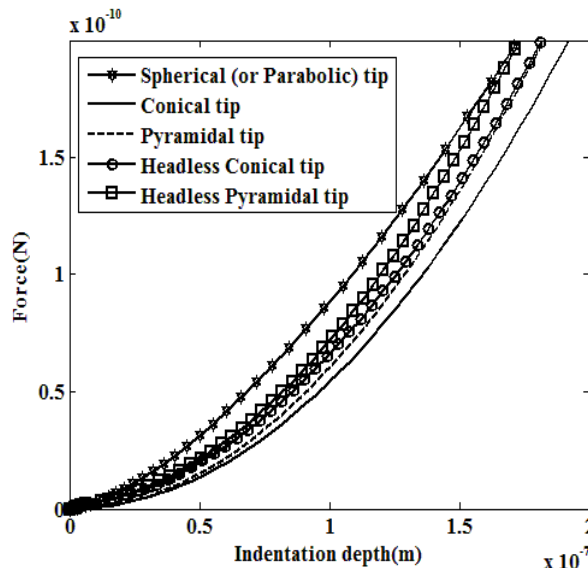
(d): Comparison of the three classes
Fig. 7 Force- indentation depth simulation with different tips for the yeast cell.



(c): Pyramidal class

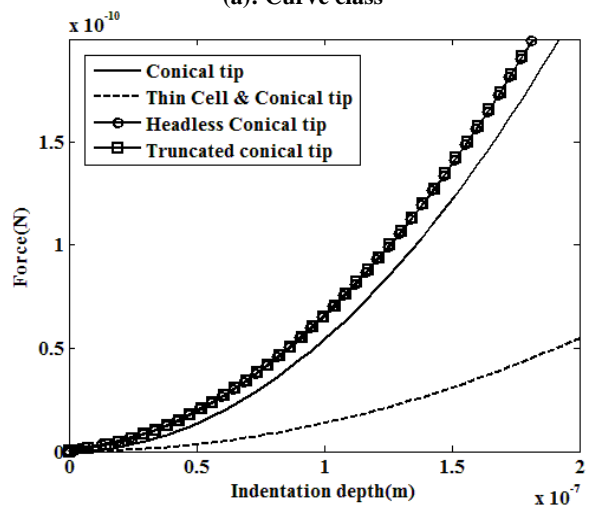


(a): Curve class



(d): Comparison of the three classes

Fig. 8 Force- indentation depth simulation with different tips for the mouse embryonic cell.



(b): Conical class

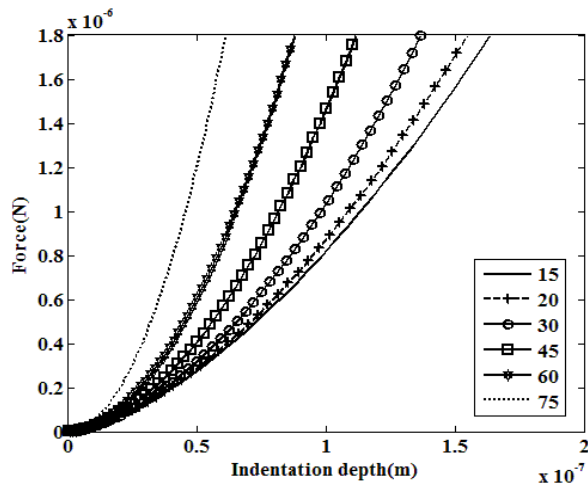
Table 1 Applied particle's properties

	PaE_p	ν_p	μmR_p
Gold Nano particle	85.2 G	0.42	0.01
Yeast cell	150 M	0.5	4
Mouse embryonic cell	17.8 k	0.5	12

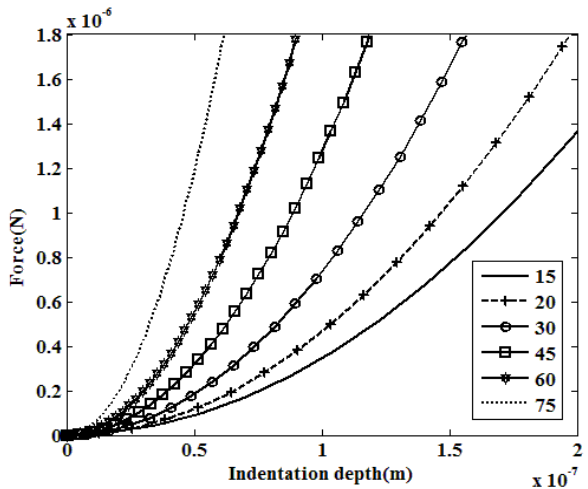
It should be mentioned that in the following, whenever spherical, conical and pyramidal words are used it refers to their tips unless it is followed by other words. In both biological cells, the force- indentation depth curve for

the hyperbolic type is positioned at the highest level and the spherical one at the lowest level. The spherical one (also parabolic) was so near to the spherical for thin sample. In the second class (conical class), the blunted cone and the truncated cone were so close to each other and positioned at the highest level. The cone has a near prediction to blunted and truncated cones. But, after considering the particle thickness in the theory, a significant difference was observed between cone for a thin sample and the regular cone. In the third class, all of pyramidal tips have near predictions. Finally, general comparison between these three classes shows that the curve class, pyramidal class and conical class have highest to lowest curves, respectively. In all of the simulations which have been done in this paper until now, the semi vertical angel was assumed about 20 degrees.

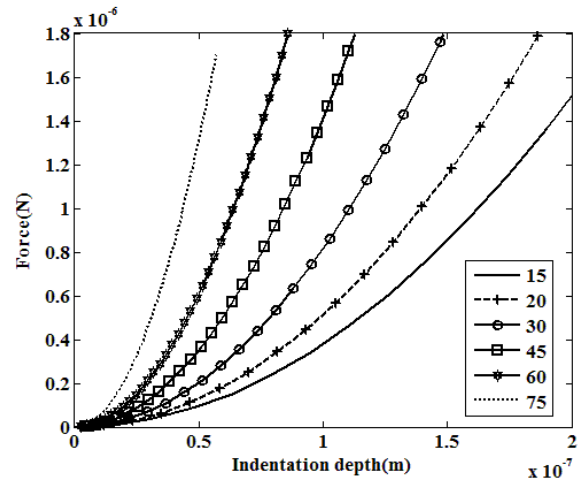
In hyperbolic, conical and pyramidal tips, this angle is an important parameter. So to observe its effect, force-indentation depth curves and indentation of different values of this parameter will be simulated for yeast and mouse embryonic cells, “Figs. 9 and 10”.



(a): Hyperbolic tip

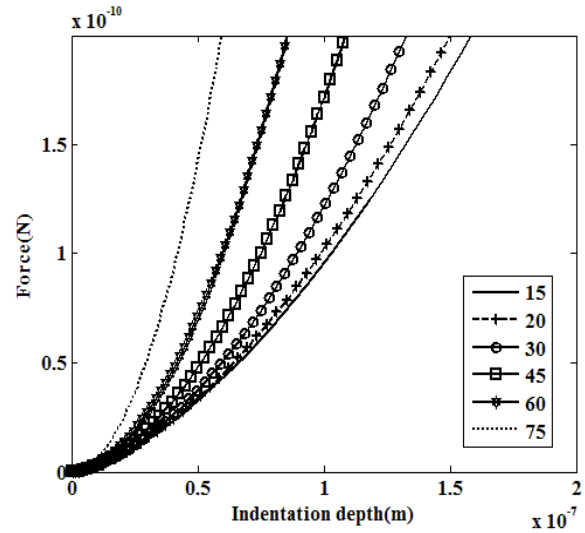


(b): Conical tip

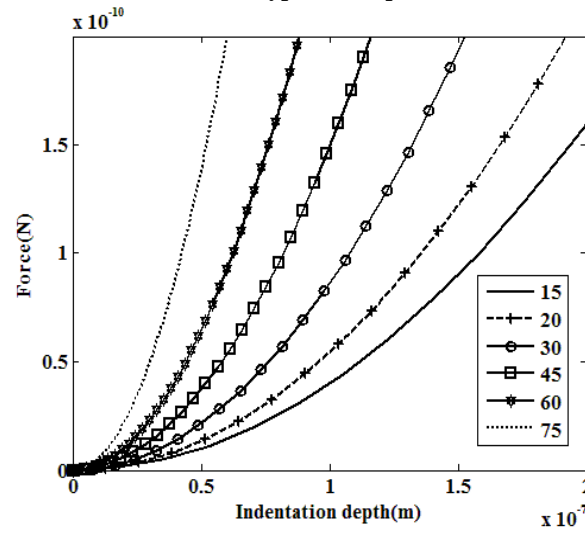


(c): Pyramidal tip

Fig. 9 Investigation of the effect of the semi vertical angle in force- indentation depth simulation of the yeast cell.



(a): Hyperbolic tip



(b): Conical tip

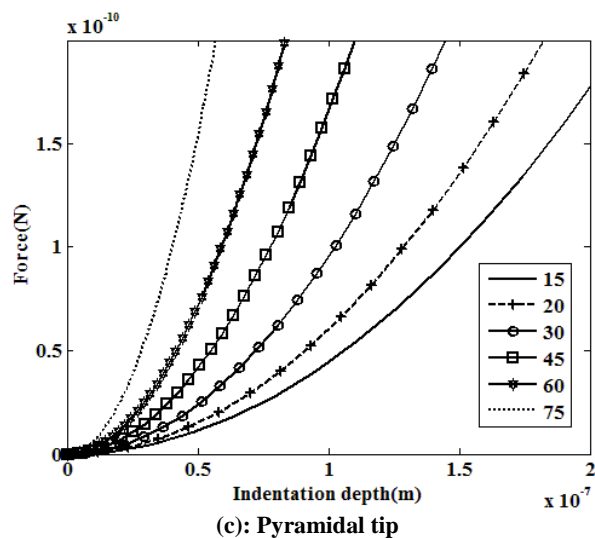


Fig. 10 Investigation of the effect of the semi vertical angle in force- indentation depth simulation of the mouse embryonic cell.

According to “Figs. 9 and 10”, it can be said that in all of studied geometries and for both cells, increasing of the semi vertical angel results in higher curves. This means that for an equal indentation depth, the geometry with higher semi vertical angel needs to apply more force and consequently in the case of biological cell higher angels damage the sample more. Similar results have been obtained for an isobutadiene rubber which has been indented by a conical tip, “Fig. 11”, [12].

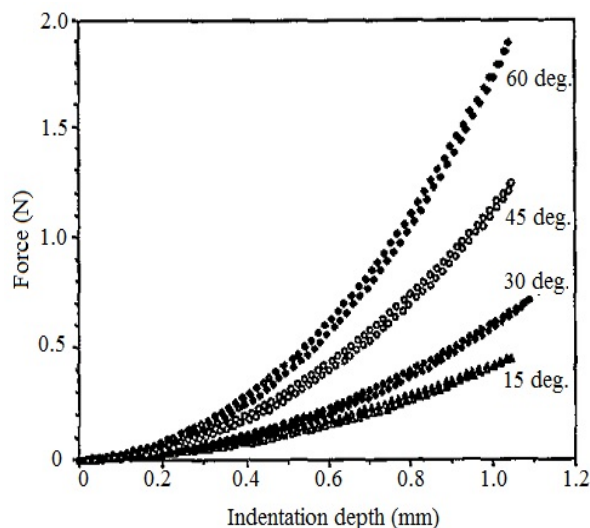


Fig. 11 Investigating of the effect of the semi vertical angel on the indentation of the poly iso-butadiene rubber by a conical tip [12].

Similar results were also obtained by Wagih and Fathy doing experimental research and FE simulation for the indentation of Aluminium Nano-composites [24]. The

same observation is concluded for the indentation of Nano-composites in [24].

Finally, it can be concluded that the best tip for biological cells is simple conical tip which inserts less force. Also, lower semi vertical angles of this tip have less applied force on biological cells and consequently less damage will be induced.

4 CONCLUSION

In a comprehensive research using numerical simulation, effects of the geometrical parameters of different tips were investigated. Since existing theories have used some simplifying assumptions (rigidity of the tip and small radius in comparison with the sample), they were corrected to be more general for any kind of particles (even biological cells). Force- indentation depth simulation has been done for the gold Nano particle and according to the observed results, eliminating simplifying assumptions avoids big errors in calculations of samples’ elasticity module and the prediction of their behavior in force- indentation depth curves.

After that, different tip’s geometries, the biological cell and finally effective geometrical parameters of samples and tips were investigated simultaneously to observe which kind of tips and geometries have less damage on biological cells. Simulations were done for mouse embryonic and yeast cells. For both cells, in general, curve class, pyramidal class and finally conical class positioned at the highest to lowest levels respectively. In the hyperbolic, conical and pyramidal tips, the important parameter was semi vertical angel which was simulated with different magnitudes to observe its effect. The observed results for three investigated geometries showed that for both cells, increasing of the semi vertical angel leads to higher curves which shows the necessity of the higher force and consequently more damage for the cell.

REFERENCES

- [1] Discher, D., Dong, C., Fredberg, J. J., Guilak, F., Ingber, D., Janmey, P., Kamm, R. D., Schmid-Schönbein, G. W., and Weinbaum, S., Cell Research and Applications for the Next Decade, *Annals of Biomedical Engineering*, Vol. 37, No. 5, 2009, pp. 847-859, DOI: 10.1007/s10439-009-9661-x.
- [2] Alonso, J. L., Goldmann, W. H., Feeling The Forces, *Atomic Force Microscopy in Cell Biology*, Life Sciences, Vol. 72, No. 23, 2003 pp. 2553-2560, DOI: 10.1016/S0024-3205(03)00165-6.
- [3] Lin, D. C., Dimitridas, E. K., and Horkay, F., Robust Strategies for Automated AFM Force Curve Analysis-I.

- Non-Adhesive Indentation of Soft, Inhomogeneous Materials, *ASME*, Vol. 129, No. 3, 2007, pp. 430-440, DOI: 10.1115/1.2720924.
- [4] Kuznetsova, T. G., Starodubtseva, M. N., Yegorenkov, N. I., Chizhik, S. A., and Zhdanov, R. I., *Atomic Force Microscopy Probing of Cell Elasticity*, *Micron*, Vol. 38, No. 8, 2007, pp. 824-33, DOI: 10.1016/j.micron.2007.06.011.
- [5] Rico, F., Roca-Cusachs, P., Gavara, N., Farré, R., Rotger, M., and Navajas, D., *Probing Mechanical Properties of Living Cells by Atomic Force Microscopy with Blunted Pyramidal Cantilever Tips*, *Physical Review*, Vol. 72, No. 2, 2005, pp. e021914, DOI: 10.1103/PhysRevE.72.021914.
- [6] Rosenbluth, M. J., Lam, W. A., and Fletcher, D. A., *Force Microscopy of Nonadherent Cells: A Comparison of Leukemia Cell Deformability*, *Biophysical*, Vol. 90, No. 8, 2006, pp. 2994-3003, DOI: 10.1529/biophysj.105.067496.
- [7] Krieg, M., Arboleda-Estudillo, Y., Puech, P. H., Käfer, J., Graner, F., Müller, D. J., and Heisenberg, C. P., *Tensile Forces Govern Germ-Layer Organization in Zebra Fish*, *Nature Cell Biology*, Vol. 10, 2008, pp. 429-436, DOI: 10.1038/ncb1705.
- [8] Park, S., Yong, J. L., *Nano-Mechanical Compliance of Müller Cells Investigated by Atomic Force Microscopy*, *International Journal of Biological Sciences*, Vol. 9 No. 7, 2013, pp. 702-708, DOI: 10.7150/ijbs.6473.
- [9] Wenger, M. P. E., Bozec, L., Horton, M. A., and Mesquida, P., *Mechanical Properties of Collagen Fibrils*, *Biophysical Journal*, Vol. 93, No. 4, 2007, pp.1255-1263, DOI: 10.1529/biophysj.106.103192.
- [10] Touhami, A., Nysten, B., and Dufrière, Y. F., *Nanoscale Mapping of the Elasticity of Microbial Cells by Atomic Force Microscopy*, *Langmuir*, Vol. 19, NO. 11, 2003, pp. 4539-4543, DOI: 10.1021/la034136x.
- [11] Bilodeau, G. G., *Regular Pyramid Punch Problem*, *ASME Journal of Applied Mechanics*, Vol. 59, No. 3, 1992, pp. 519-523, DOI: 10.1115/1.2893754.
- [12] Briscoet, B. J., Sebastian, K. S., and Adams, M. J., *The Effect of Indenter Geometry On the Elastic Response to Indentation*, *Journal of Physics D: Applied Physics*, Vol. 27, No. 6, 1994, pp. 11561162, DOI: 10.1088/0022-3727/27/6/013.
- [13] Akhremitchev, B. B., Walker, G. C., *Finite Sample Thickness Effects on Elasticity Determination Using Atomic Force Microscopy*, *Langmuir*, Vol. 15, No. 17, 1999, pp. 5630-5634, DOI: 10.1021/la980585z.
- [14] Dimitriadis, E. K., Horkay, F., Maresca, J., Kachar, B., and Chadwick, R. S., *Determination of Elastic Moduli of Thin Layers of Soft Material Using the Atomic Force Microscope*, *Biophysical Journal*, Vol. 82, No. 5, 2002, pp. 2798–2810, DOI: 10.1016/S0006-3495(02)75620-8.
- [15] Gavara, N., Chadwick, R. S., *Determination of the Elastic Moduli of Thin Samples and Adherent Cells Using Conical AFM Tips*, *Nature Nanotechnology*, Vol. 7, No. 11, 2012, pp. 733–736, DOI: 10.1038/nnano.2012.163.
- [16] Rico, F., Roca-Cusachs, P., Gavara, N., Farré, R., Rotger, M., and Navajas, D., *Probing Mechanical Properties of Living Cells by Atomic Force Microscopy with Blunted Pyramidal Cantilever Tips*, *Physical Review E*, Vol. 72, 2005, pp. 021914, DOI: 10.1103/PhysRevE.72.021914.
- [17] Park, S., Koch, D., Cardenas, R., Kas, J., and Shih, C. K., *Cell Motility and Local Viscoelasticity of Fibroblasts*, *Biophysics Journal*, Vol. 89, No. 6, 2005, pp. 4330-42, DOI: 10.1529/biophysj.104.053462.
- [18] JPK Instruments, *Determining the Elastic Modulus of Biological Samples Using Atomic Force Microscopy*, JPK application Note, www.jpk.com, 2014.
- [19] Wagih, A., Maimí, P., Blanco, N., and Trias, D., *Predictive Model for The Spherical Indentation of Composite Laminates with Finite Thickness*, *Composite Structures*, Vol. 153, 2016, pp. 468–477, DOI: 10.1016/j.compstruct.2016.06.056.
- [20] Turner, J. R., *Contact on a Transversely Isotropic Half-Space or Between Two Transversely Isotropic Bodies*, *International Journal of Solids and Structures*, Vol. 16, No. 5, 1980, pp. 409–19, DOI: 10.1016/0020-7683(80)90039-6.
- [21] Hertz, H., *Über Die Berührung Fester Elastischer Körper*, *Journal für Die Reine und Angewandte Mathematik*, Vol. 92, 1882, pp. 156-171, DOI: 10.1515/crll.1882.92.156.
- [22] Harding, J. W., Sneddon, I. N., *The Elastic Stresses Produced by The Indentation of the Plane Surface of a Semi-Infinite Elastic Solid by A Rigid Punch*, *Mathematical Proceedings of the Cambridge Philosophical Society*, Vol. 41, No. 1, 1945, pp. 16-26, DOI: 10.1017/S0305004100022325.
- [23] Reifengerger, R., *Fundamentals of Atomic Force Microscopy Part I: Foundations*, World Scientific Publishing Co, London, GB, 2016, pp. 141-146, ISBN: 978-9814630344.
- [24] Wagih A., Fathy A., *Experimental Investigation and Fe Simulation of Nanoindentation on Al-Al2O3 Nanocomposites*, *Advanced Powder Technology*, Vol. 27, No. 2, 2016, 403–410, DOI: 10.1016/j.apt.2016.01.021.